ADVANCED MATERIALS

Supporting Information

for *Adv. Mater.*, DOI: 10.1002/adma.201906043

Unusual Two-Step Assembly of a Minimalistic Dipeptide-Based Functional Hypergelator

Priyadarshi Chakraborty, Yiming Tang, Tomoya Yamamoto, Yifei Yao, Tom Guterman, Shai Zilberzwige-Tal, Nofar Adadi, Wei Ji, Tal Dvir, Ayyalusamy Ramamoorthy, Guanghong Wei, and Ehud Gazit**

Supporting Information

Unusual two-step assembly of a minimalistic dipeptide-based functional hypergelator

Priyadarshi Chakraborty, Yiming Tang, Tomoya Yamamoto, Yifei Yao, Tom Guterman, Shai Zilberzwige-Tal, Nofar Adadi, Wei Ji, Tal Dvir, Ayyalusamy Ramamoorthy, Guanghong Wei and Ehud Gazit**

Dr. Priyadarshi Chakraborty, Tom Guterman, Shai Zilberzwige-Tal, Dr. Wei Ji, Prof. Tal Dvir, Prof. Ehud Gazit
School of Molecular Cell Biology and Biotechnology
George S. Wise Faculty of Life Sciences
Tel Aviv University
Tel Aviv 6997801, Israel
E-mail: ehudg@post.tau.ac.il

Yiming Tang, Yifei Yao, Prof. Guanghong Wei
Department of Physics,
State Key Laboratory of Surface Physics,
Key Laboratory for Computational Physical Sciences (MOE),
Fudan University,
Shanghai, 200433, People's Republic of China.
E-mail: ghwei@fudan.edu.cn

Dr. Tomoya Yamamoto, Prof. Ayyalusamy Ramamoorthy
Biophysics and Department of Chemistry, Biomedical Engineering, Macromolecular Science and Engineering,
University of Michigan
Ann Arbor, Michigan 48109, United States

Nofar Adadi, Prof. Tal Dvir, Prof. Ehud Gazit
Department of Materials Science and Engineering
Iby and Aladar Fleischman Faculty of Engineering
Tel Aviv University
Tel Aviv 6997801, Israel

Experimental section

*Preparation of Hydrogel/Assembly***:** All peptides used in this work were purhchased from GL Biochem, Shanghai. Self-assembled nanostructures or hydrogels were prepared by a solvent-switch technique. Lyophilized peptides were dissolved in DMSO at a concentration of 100 mg mL^{-1}. The hydrogels/assemblies were prepared by diluting this stock solution in ultrapure water (Biological Industries, Beit Haemeck, Israel). To prepare the composite hydrogels with polyaniline (peptide-PAni), the required quantity of aniline (Ani) (ACS reagent, Sigma-Aldrich) was first homogeneously solubilized in water by rigorous vortexing. The Fmoc-Lys(Fmoc)-Asp stock solution was then diluted in this aqueous solution of Ani yielding a Ani containing hydrogel with different molar ratios of peptide and Ani (1:5, 1:10 and 1:15). The final peptide concentration was 0.5 wt%. Ani was then *in situ* polymerized by an aqueous solution of ammonium persulfate (APS) (Sigma-Aldrich, molar ratio of APS: Ani = 1.5:1). The color of the hydrogels turned dark green with the course of polymerization indicating the formation of polyaniline (PAni) inside the hydrogels.

High-Resolution Scanning Electron Microscopy (HR-SEM): The samples were prepared by drop casting on siliconized glass and drying in room temperature overnight. The samples were sputtered with Cr and imaged using a JSM-6700F high-resolution field emission SEM (Jeol, Japan), operating at an acceleration voltage of 10 kV.

Transmission electron microscopy (TEM): Hydrogels samples of 10 µL were drop casted onto 400-mesh copper grids covered by a carbon-stabilized Formvar film (SPI, West Chester, PA, USA). The samples were dried under ambient conditions and the micrographs were recorded using a JEM-1400Plus Transmission Electron Microscope (JEM) operating at 80 kV.

Fourier-transform infrared spectroscopy (FTIR) spectroscopy: To obtain the FTIR spectra, 30 µL of the hydrogels were deposited onto disposable KBr infrared sample cards (Sigma-Aldrich, Rehovot, Israel), which were then allowed to dry under vacuum. The measurements were

carried out in a nitrogen purged Nexus 470 FTIR spectrometer (Nicolet, Offenbach, Germany) equipped with a deuterated triglycine sulfate (DTGS) detector.

Rheology: Mechanical properties of the hydrogels were measured on an ARES-G2 rheometer (TA Instruments, New Castle, DE, USA) using a 20 mm parallel-plate geometry with a gap of 1000 µm. Sheer recovery was explored by the step strain method, with time sweep steps successively carried out at 0.1% and 200% strain.

Powder X-ray diffraction: Powder X-ray diffraction patterns of the dried hydrogels were collected by using a BRUKER d8 ADVANCE DIFFRACTOMETER equipped with Goebels mirrors to parallelize the beam and LYNXEYE-XE linear detector.

UV-Vis spectra: UV-Vis spectra of the samples were recorded in a T60 UV-Vis spectrophotometer (PG instruments). A quartz cuvette with an optical path length of 1 mm was used. To obtain the UV-Vis spectra of Peptide-PAni composite hydrogels, a pre-prepared hydrogel was dispersed in ddH_2O.

Fluorescence spectroscopy: Fluorescence spectra of the hydrogels were recorded using a Horiba fluoromax 4 instrument. The hydrogels were prepared in quartz cells of 1 cm path length and excited at 280 nm. Emission scans were recorded using 3 nm excitation and emission slits.

Solid state NMR: Cross-polarization (CP)-MAS NMR experiments were performed on a Bruker 400 MHz NMR spectrometer using a 2.5 mm MAS probe. ^{1}H and ^{13}C NMR resonance frequencies were 400.11 MHz and 100.62 MHz, respectively. ^{13}C ramped-CPMAS NMR spectra[1,2] were recorded under 15 kHz MAS with a 3.0 ms of CP-contact time. Proton decoupling during ^{13}C signal acquisition was achieved by the SPINAL-64 decoupling pulse sequence[3] with a radio-field (RF) frequency field strength of 104 kHz. The ^{13}C chemical shifts were referenced using the chemical shift value observed for a adamantane-KBr powder sample:

δ_{iso} = 29.5 ppm (for methine carbon) with respect to the chemical shift value for TMS (δ_{iso} = 0 ppm).

For the samples used in CPMAS NMR experiments, a stock solution of Fmoc-Lys(Fmoc)-Asp in DMSO-d_6 (100mg/mL) was added to MilliQ water, where the final concentration of Fmoc-Lys(Fmoc)-Asp was 0.5 wt%. After the incubation for 10 min, 1 h or 2.5 h, samples were frozen in liquid nitrogen, followed by lyophilization for more than 48 hours. For the 10 min lyophilized dipeptide sample, adamantane was added to the powder as an internal chemical shift reference. The lyophilized powder sample was packed into a 2.5 mm MAS rotor for CPMAS NMR experiments. The powder samples were stored at -20 °C before carrying out NMR experiments.

Molecular dynamics: Molecular dynamics simulations have been widely used in investigating molecular details and self-assembly pathways of peptide assemblies.[4–6] In this work, microsecond-long molecular dynamics (MD) simulations on 400 Fmoc-Lys(Fmoc)-Asp molecules at different concentrations were carried out using the GROMACS package (version 2018.3)[7] in combination with the MARTINI coarse-grained (CG) model (version 2.2).[8] The mapping from all-atom model of a Fmoc-Lys(Fmoc)-Asp molecule to CG model and the interaction types of the CG beads are shown in Figure S5.

In the initial state of each simulation system at low peptide concentration, the 400 Fmoc-Lys(Fmoc)-Asp molecules were randomly placed in a 24×24×24 nm^3 cubic box containing 90000 water beads and 10000 DMSO molecules. For systems at medium and high peptide concentration, the number of Fmoc-Lys(Fmoc)-Asp molecules were kept the same (400 molecules), but the box lengths were set as 20 and 17 nm, respectively. The number of water beads were reduced to 54000 and 18000, and the corresponding numbers of DMSO molecules were 6000 and 2000, respectively. Sodium ions were added to neutralize each system.

Electrostatic interactions were treated using the Particle Mesh Ewald (PME) method, [9] with a real space cut-off of 1.2 nm. The vdW interactions were calculated using a cutoff of 1.2 nm. The solute and solvent were separately coupled to an external temperature bath using a velocity

rescaling method and a pressure bath using the Parrinello-Rahman method[10]. The temperature and pressure were maintained at 300 K and 1 bar, respectively. The neighbor-list was updated every 10 steps with a cut-off distance of 1.2 nm using a Verlet buffer.[11] The trajectory analyses were performed using in-house-developed codes and tools implemented in the GROMACS package. The fraction of solvent accessible surface area (SASA) of each group (Fmoc, Aspartic acid, and Lysine) was defined as the percentage of the SASA of that group relative to the SASA of all Fmoc-Lys(Fmoc)-Asp molecules at each time point. Two groups are considered to have atomic contact if their minimum distance is within 0.65 nm. The angle between two benzene rings refers to the angle between the normal vectors of the two rings. If the angle was larger than 90°, the supplementary angle was used as the angle between the two benzene rings. Two benzene rings are considered only if their centroid distance is within 0.8 nm. The two-dimensional free energy landscape was constructed using the relation $-RT\ln[P(\text{angle, centroid distance})]$ where P(angle, centroid distance) is the probability of a stacking pattern having a certain value of angle and centroid distance. The data in the last 0.1 μs of CG-MD trajectories were used to construct the free energy landscape. In accordance with our previous study,[12] the geometry map was plotted using RgY/RgX and RgZ/RgX as two reaction coordinates, where RgX, RgY, and RgZ are the radii of gyration (Rg) of a given nano-assembly with respect to, the three principle axes X, Y, and Z of the nanostructure respectively, in order from smallest to largest Rg values. Trajectory visualization and graphical structure analysis were performed using the Pymol software suite.[13]

XTT analysis: The hydrogels (0.1 wt%) were prepared on 96 well plates and dried under vacuum. 3T3 mouse fibroblast cells were purchased from ATCC and cultured in Dulbecco's Modified Eagle's Medium (DMEM) supplemented with 10 wt% fetal calf serum, 100 U mL^{-1} penicillin, 100 U mL^{-1} streptomycin, and 2 mmol L^{-1} L-glutamine (all from Biological Industries, Israel). The cells were cultured in a petri dish at 37 °C in a humidified atmosphere containing 5% CO_2. 3T3 fibrobalsts (2×10^5 cells/mL) were seeded on the dried hydrogel fibers and cell viability

was assessed by XTT analysis after particular time intervals. Cell viability was evaluated using the XTT cell proliferation assay kit (Biological Industries) according to the manufacturer's instructions. Briefly, 100 µL of the activation reagent was added to 5 mL of the XTT reagent, followed by the addition of 100 µL of activated XTT solution to each well. After 2.5 h of incubation at 37°C, color intensity was measured using an enzyme-linked immunosorbent assay (ELISA) microplate reader at 450 and 630 nm. Results are presented as means ± SEM. Each experiment was repeated three times.

2D and 3D cell culture: 3T3 mouse fibroblast cells were purchased from ATCC and cultured in Dulbecco's Modified Eagle's Medium (DMEM) supplemented with 10% fetal calf serum, 100 U mL^{-1} penicillin, 100 U mL^{-1} streptomycin, and 2 mmol L^{-1} L-glutamine (all from Biological Industries, Israel). The cells were cultured in a petri dish at 37 °C in a humidified atmosphere containing 5% CO_2. Fmoc-Lys(Fmoc)-Asp hydrogels were prepared in a 24 well-plate and repeatedly washed for three times with culture medium to ensure complete removal of excess materials followed by UV sterilization. Subsequently, before seeding the cells, the pH of the final medium over the gels was measured to be 7.4-7.8, indicating a suitable pH for cell culture. After reaching a confluence of 90%, the cells were separated from the petri dish using trypsin A and 60,000 cells in 0.2 ml of fresh culture medium were seeded per well, on the pre-washed gel samples, and incubated for 1, and 4 days. A fluorescent Live/Dead staining assay (Sigma Aldrich) containing fluorescein diacetate (6.6 µg/ml) and propidium iodide (5 µg/ml) was used to visualize the proportion of viable versus non-viable cells. The labelled cells were immediately viewed using a Nikon Eclipse Tifluorescent microscope and images were captured by a ZylascMOS camera using Nikon Intensilight C-HGFI fluorescent lamp. In order to evaluate cell migration, 3T3-seeded duplicate gel samples at the 4 day time-point was studied by a scanning laser confocal microscope (Nikon Eclipse Ni). For confocal imaging, the cells were stained with fluorescein diacetate (6.6 µg/ml) and propidium iodide (5 µg/ml).

Current-voltage (I–V) measurements: The peptide-PAni hydrogels were drop-casted on pre-fabricated field-effect transistor substrates (Ossila, UK) with an electrode gap of 2 μm and dried under ambient conditions. Current-voltage (*I–V*) measurements were performed on a Keithley 4200-SCS source-meter using the two-probe method. All measurements were carried out from -1 V to 1 V with 0.05 V steps, and 0.1 s hold time and sweep delay.

DNA binding study: The interactions between plasmid DNA (pDNA) and peptide-PAni hydrogel were detected by absorbance measurements. A total of 500μL pDNA (pET14b-eGFP) (10 μg mL^{-1}) were transferred to the wells of 24 plate containing the composite peptide-PAni hydrogels (molar ratio of peptide: Ani = 1:10). An aliquot of 1μL was taken at defined times from each well to measure pDNA concentration using Nano-Drop (Nano drop one, Thermo scientific). The experiement was repeated three times and the data represents the average of them.

Table S1. Comparison of CGC values of different class of hydrogelators.

Category of hydrogelators	Specific sub-category of hydrogelators	CGC (wt%)	Reference
Small molecule-based	Pyridine-based	0.12	[14]
	C_3 symmetry-based	0.033	[15]
	Rigid aliphatics	0.02	[16]
	Bolalipids	0.01	[17]
Peptide-based	Cyclic tri-β-peptide	0.006	[18]
	FEFEFKFKFEFEFKFK	0.007	[19]
Amino acid-based	With Alkyl side chain	0.05	[20]
	With aromatic group	0.1	[21]
Peptide derivatives	Capped N or C terminus	0.01	[22–24]
	Containing alkyl/lipid chains	0.25	[25,26]
	With aromatic groups	0.01	[27]
Saccharide-based	Mono saccharide based	0.07	[28]
	Oligo saccharide based	1	[29,30]

Note S1

We divided hydrogelators into 5 broad categories.[31] Each of these categories were subsequently divided into specific sub-categories. The hydrogelators having the lowest CGC amongst these sub-categories is noted in Table S1.

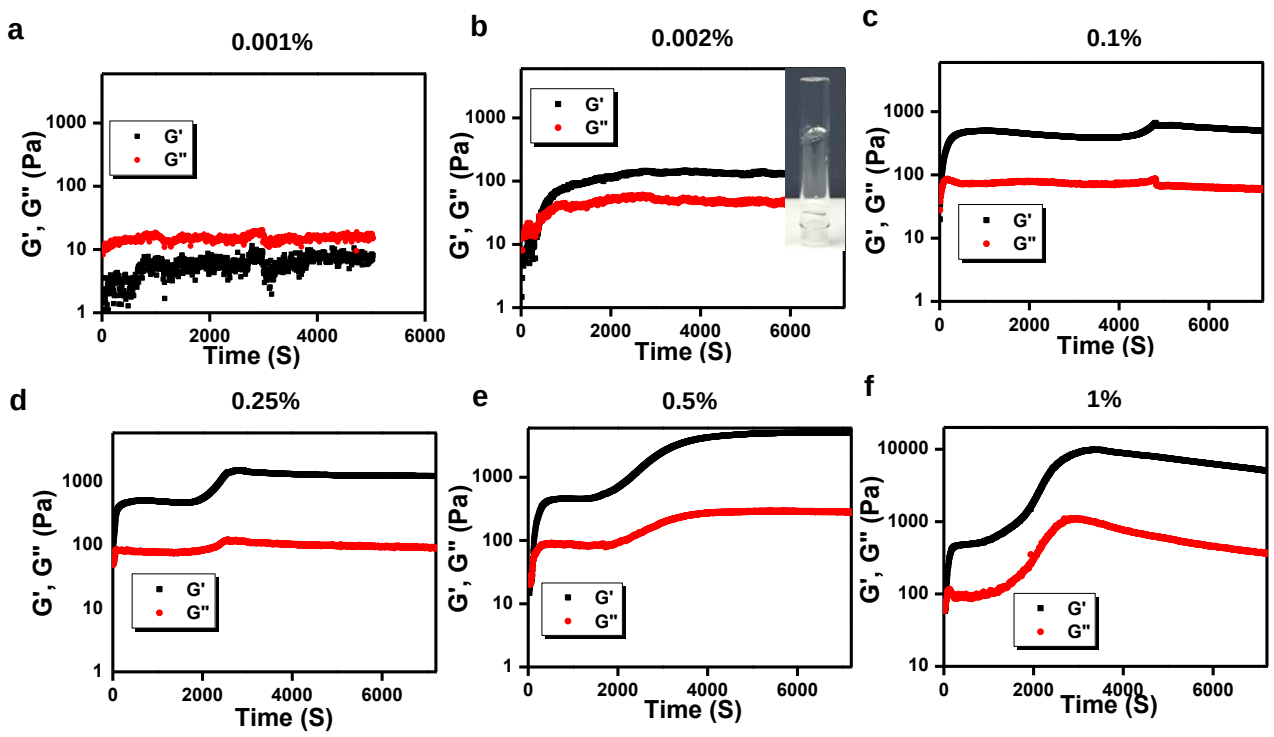

Figure S1. **Time dpendent evolution of the G' and G" at a constant frequency of 1 Hz**. Time sweep experiement carried on the Fmoc-Lys(Fmoc)-Asp hydrogels/solutions at (a) 0.001 wt%, (b) 0.002 wt% (Inset: Optical image of the 0.002 wt % hydrogel), (c) 0.1 wt%, (d) 0.25 wt%, (e) 0.5 wt% , (f) 1 wt% concentration.

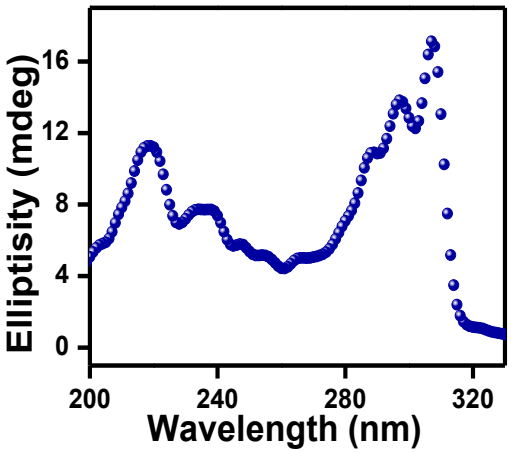

Figure S2. CD spectra of the Fmoc-Lys(Fmoc)-Asp hydrogels (0.5 wt%).

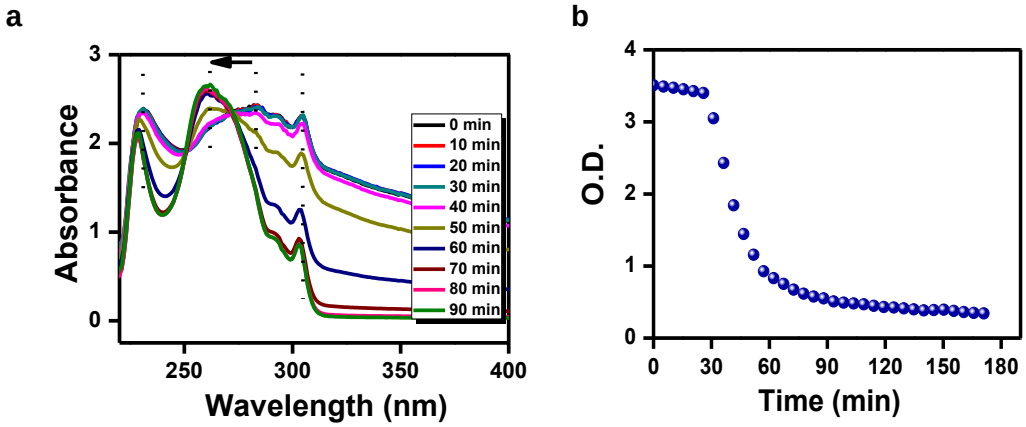

Figure S3. Spectroscopic characterization of the Fmoc-Lys(Fmoc)-Asp hydrogel formation. (a)Time dpendent UV-Vis spectra of a 0.1 wt% Fmoc-Lys(Fmoc)-Asp hydrogel. (b) Time dependent reduction of the O.D. values of a 0.5 wt% hydrogel indicating decreasing turbidity with time.

Note S2

The 231 nm and 283 nm absorbance peaks can be ascribed to n-π* and π-π* transition of Fmoc-Lys(Fmoc)-Asp, respectively. The fact that the 231 nm peak decreased in absorbance intensity, whereas, the 283 nm peak increased over time suggests that the probability of n-π* transition decreased during self-assembly, while the probability of π-π* transition increased.[32]

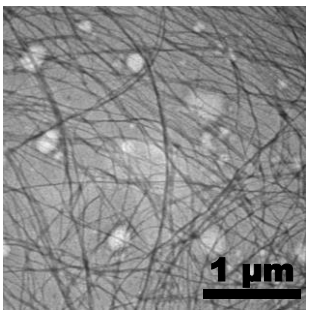

Figure S4. TEM micrograph of a ~ 3 month aged Fmoc-Lys(Fmoc)-Asp hydrogel.

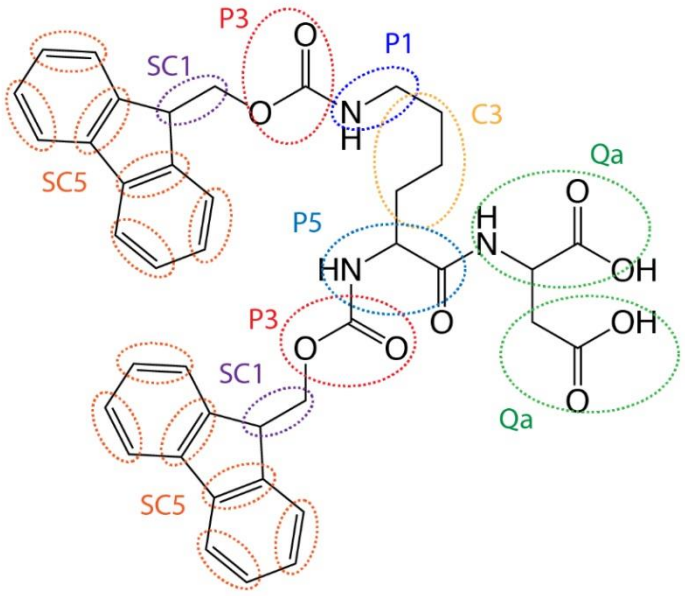

Figure S5. Mapping from all-atom model of Fmoc-Lys(Fmoc)-Asp molecule to coarse-grained model. The atoms in each circle are mapped to one coarse-grained bead. The interaction type of each bead is labeled beside the circle.

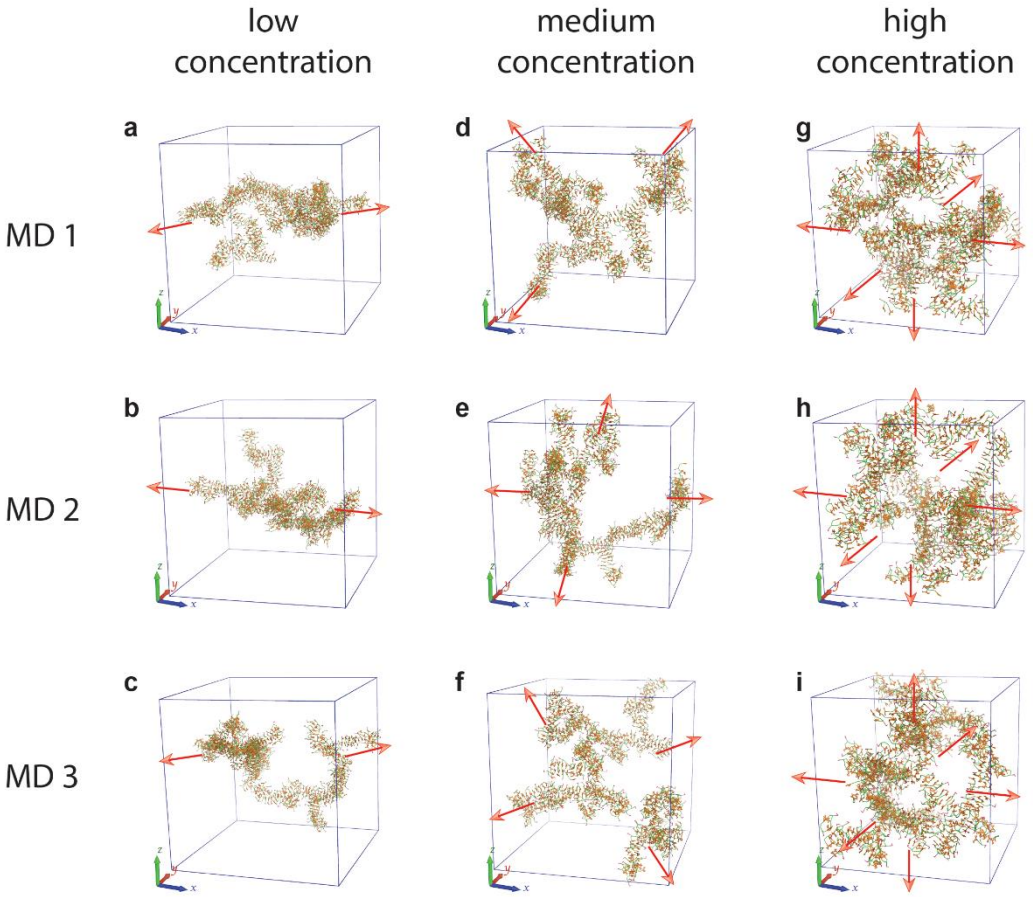

Figure S6. Structures of Fmoc-Lys(Fmoc)-Asp hydrogels at different concentrations. Three independent simulations are performed for each concentration starting from randomly dispersed Fmoc-Lys(Fmoc)-Asp molecules.

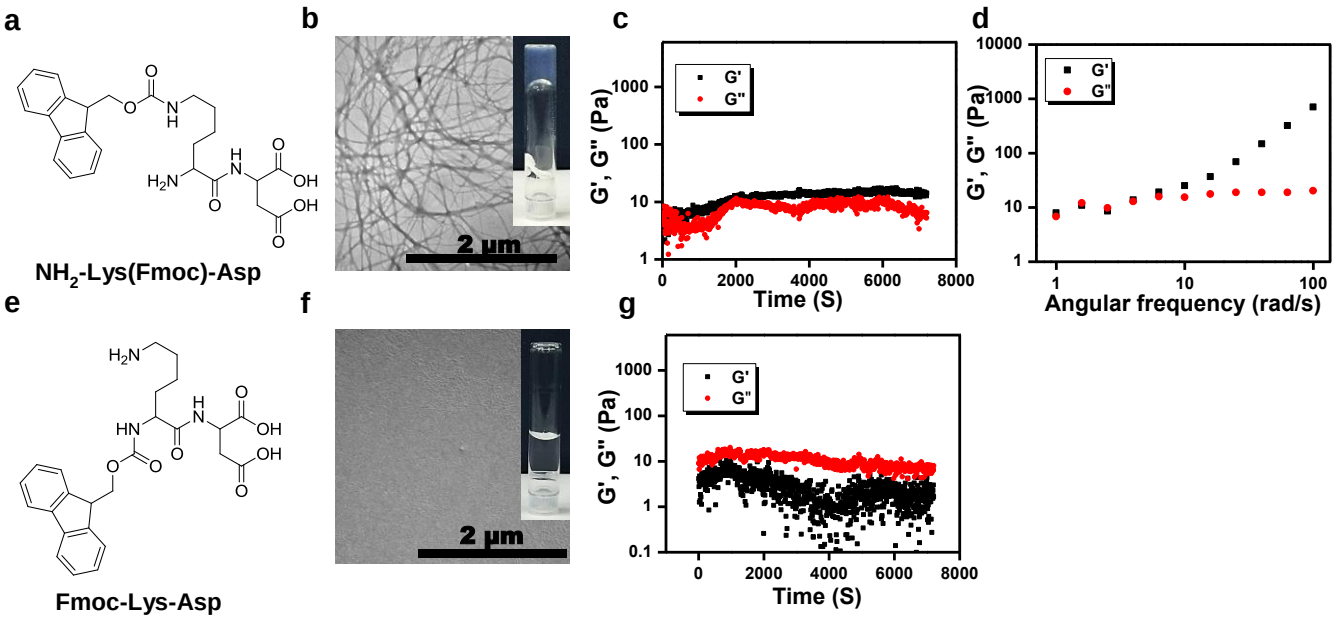

Figure S7. Characterization of the dipeptides of identical sequence but protected by a single Fmoc group (0.5 wt%). (a) Chemical structure of the dipeptide NH_2-Lys(Fmoc)-Asp. (b) TEM micrograph of the self-assembly of NH_2-Lys(Fmoc)-Asp showing fibrous architecture (Inset: optical image of a weak gel of NH_2-Lys(Fmoc)-Asp). (c) Time sweep rheology carried on the NH_2-Lys(Fmoc)-Asp (0.5 wt%) self-assembly exhibiting the G' to be higher than G". (d) Frequency dependent oscillatory rheology of the NH_2-Lys(Fmoc)-Asp self-assembly (0.5 wt%) showing a frequency dependent behaviour of the G' and G" indicating a very weak gel formation. (e) Chemical structure of the dipeptide Fmoc-Lys-Asp. (f) TEM micrograph of the self-assembly of Fmoc-Lys-Asp showing no aggregate formation (Inset: optical image of Fmoc-Lys-Asp solution showing no gelation). (g) Time sweep rheology of the Fmoc-Lys-Asp solutions (0.5 wt%) showing no gelation.

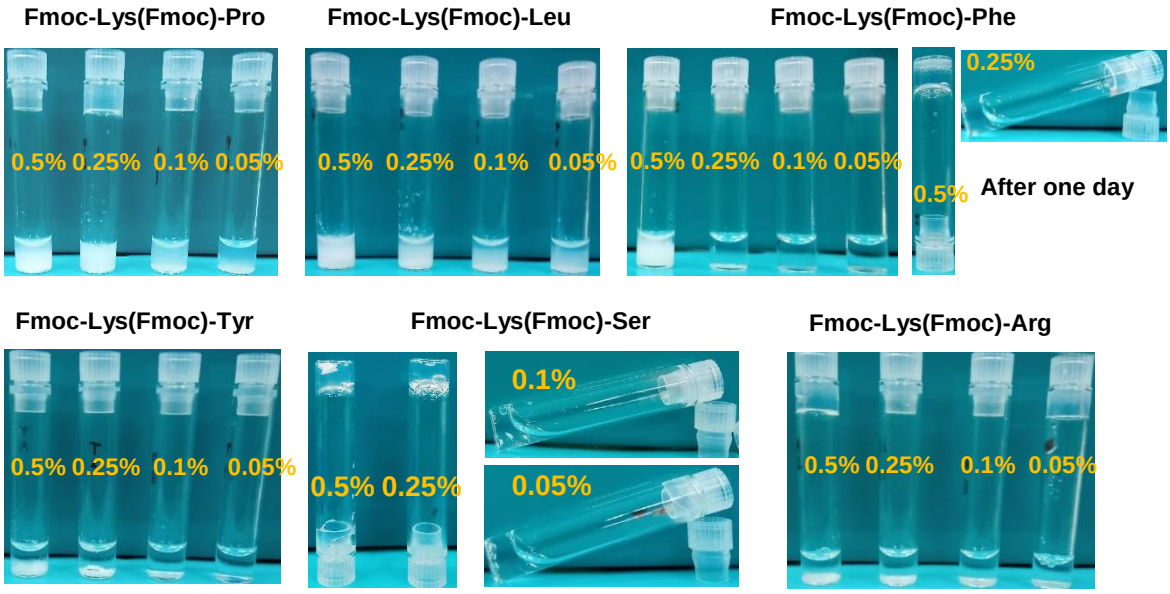

Figure S8. **Optical images of the self-assembly of the non-gelling peptides.** Although Fmoc-Lys(Fmoc)-Phe and Fmoc-Lys(Fmoc)-Ser exhibited gelation at higher concentrations, they were not homogeneous and therefore, not considered as genuine hydrogels.

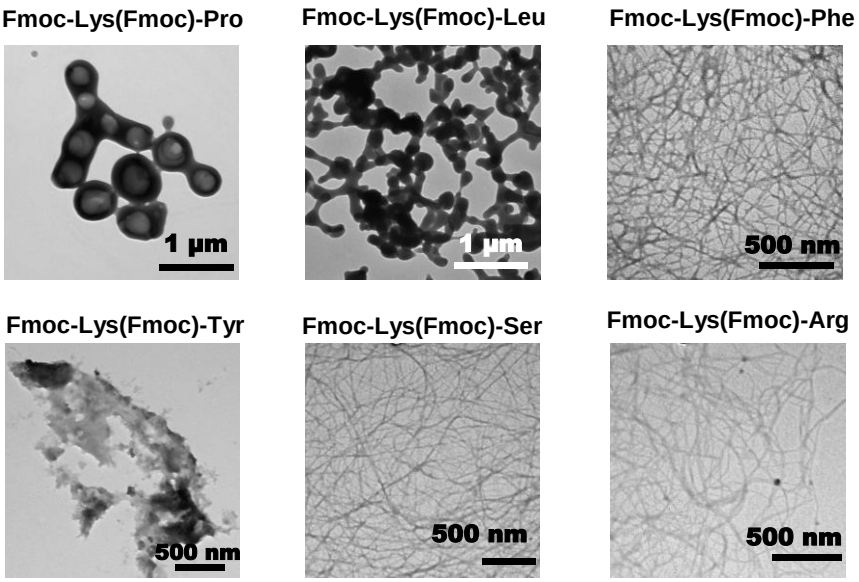

Figure S9. **TEM micrographs of the self-assembly of the non-gelling peptides.** Self assembly of non-gelling peptides exhibited diverse morphological features including, vesicles, joint vesicles, fibers and amorphous aggregates.

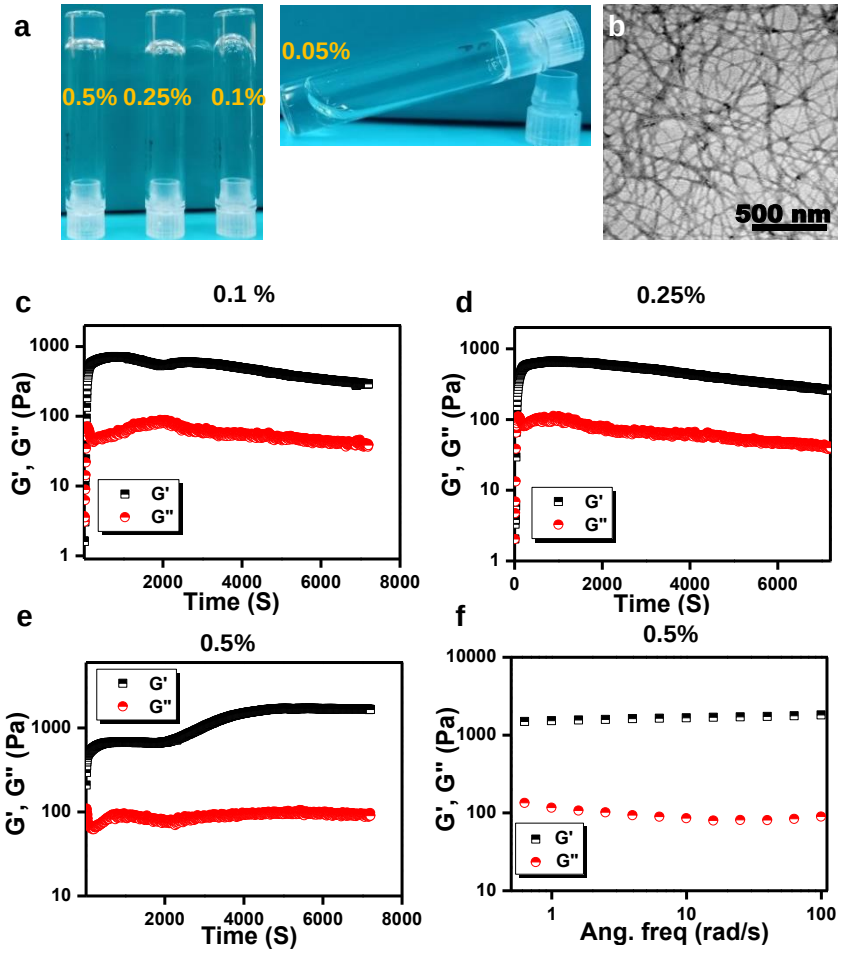

Figure S10. **Characterization of the gelling peptide Fmoc-Lys(Fmoc)-Ala.** (a) Optical image of the preparation at different concentrations exhibitng gel formation. (b) TEM micrograph of the hydrogel showing fibrous morphology. (c-e) Time sweep rheology of the hydrogels at different concentrations. Interestingly, the 0.5 wt% hydrogel exhibited the two-step growth. (f) Frequency dependent oscillatory rheology of the 0.5 wt% hydrogel.

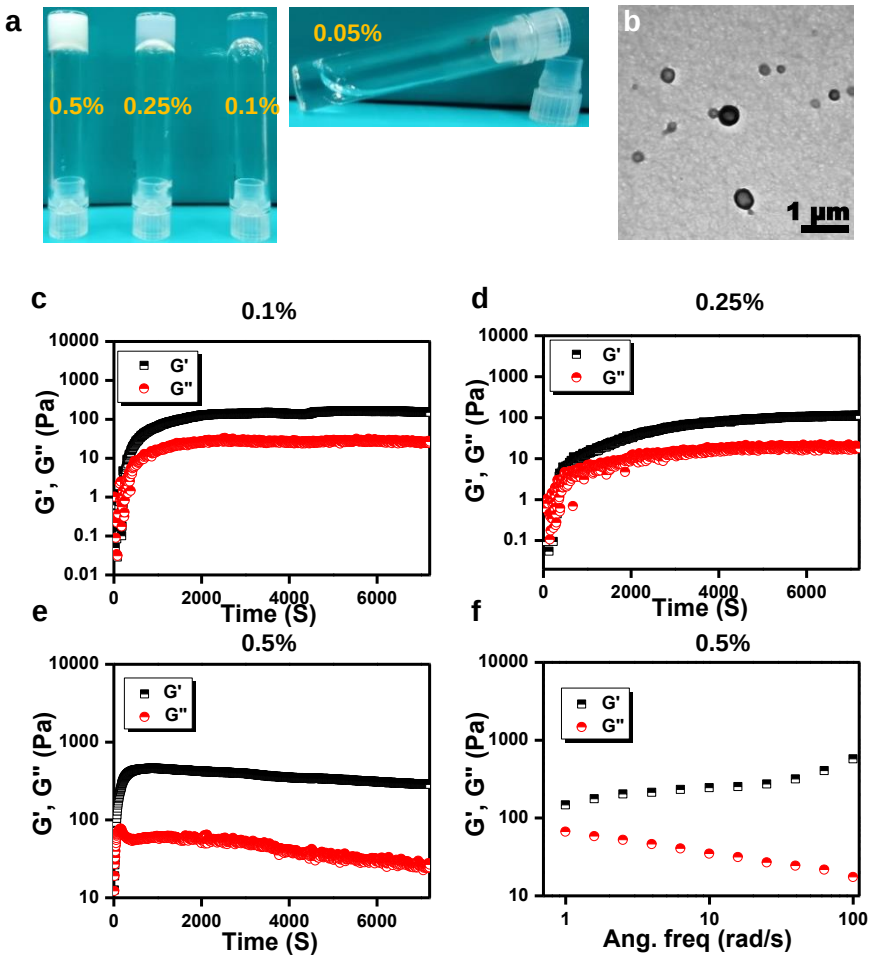

Figure S11. Characterization of the gel forming peptide Fmoc-Lys(Fmoc)-Cys. (a) Optical image of the preparation at different concentrations exhibiting gel formation. (b) TEM micrograph of the hydrogels showing fibrous morphology along with the presence of vesicles. (c-e) Time sweep rheology of the hydrogels at different concentrations. (f) Frequency dependent oscillatory rheology of the 0.5 wt% hydrogel.

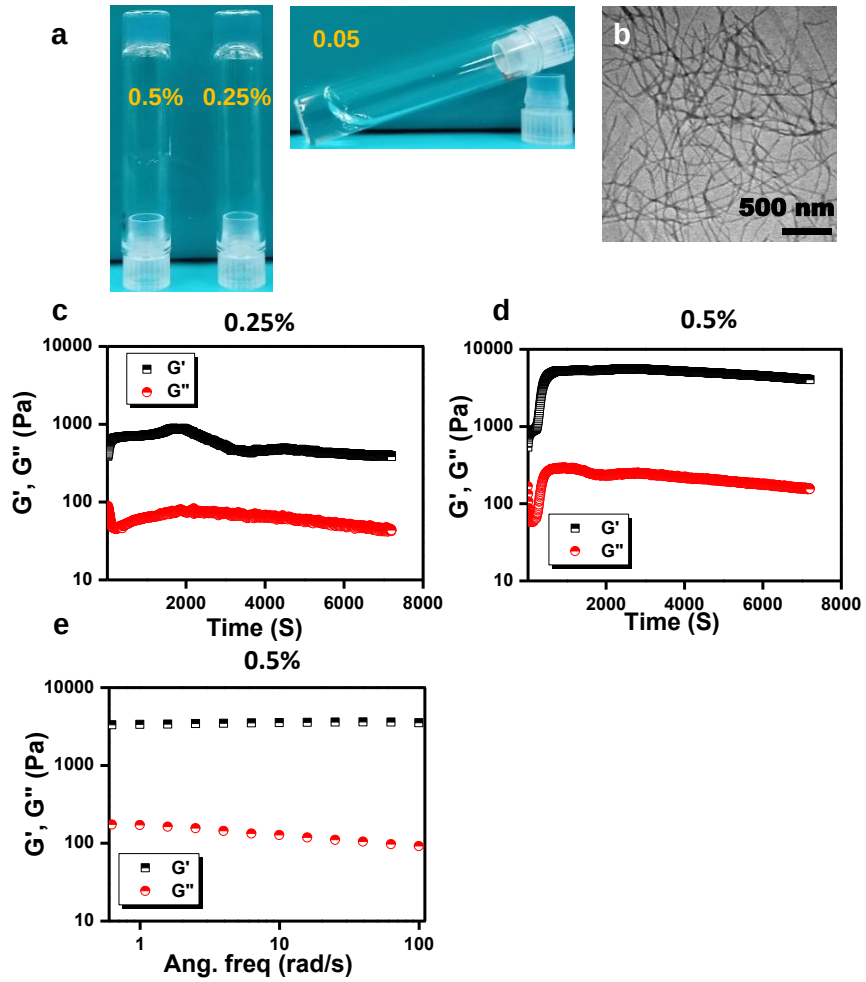

Figure S12. Characterization of the gelling peptide Fmoc-Lys(Fmoc)-Asn. (a) Optical image of the preparation at different concentrations exhibitng gel formation. (b) TEM micrograph of the hydrogels showing fibrous morphology. (c, d) Time sweep rheology of the hydrogels at different concentrations. (e) Frequency dependent oscillatory rheology of the 0.5 wt% hydrogel.

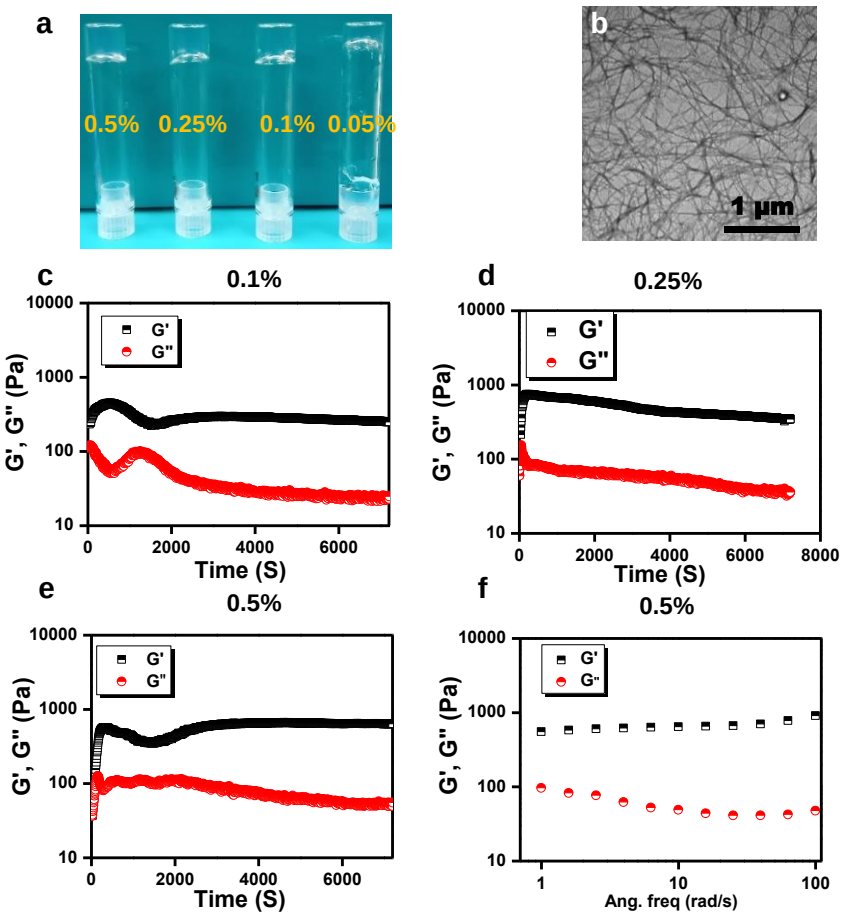

Figure S13. **Characterization of the gelling peptide Fmoc-Lys(Fmoc)-His.** (a) Optical image of the preparation at different concentrations exhibitng gel formation. (b) TEM micrograph of the hydrogels showing fibrous morphology. (c-e) Time sweep rheology of the hydrogels at different concentrations. (e) Frequency dependent oscillatory rheology of the 0.5 wt% hydrogel.

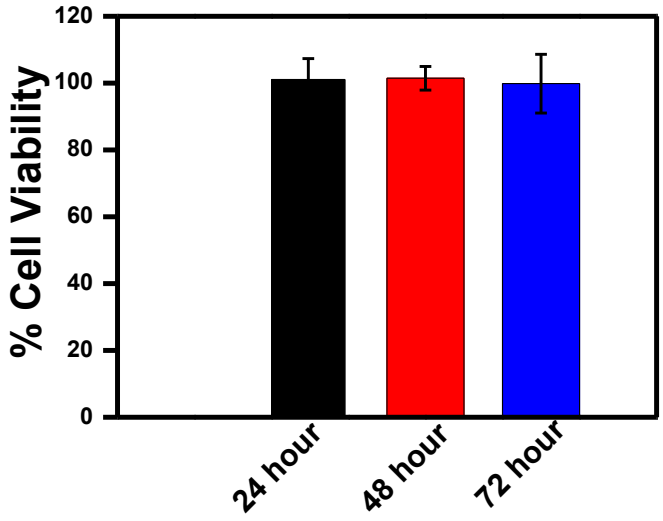

Figure S14. **Cell viability of the 0.1 wt% Fmoc-Lys(Fmoc)-Asp hydrogel fibers.** The hydrogels were prepared on 96 well plates and dried under vacuum. 3T3 fibrobalsts were seeded on the dried hydrogel fibers and cell viability was assessed by XTT analysis after particular time intervals.

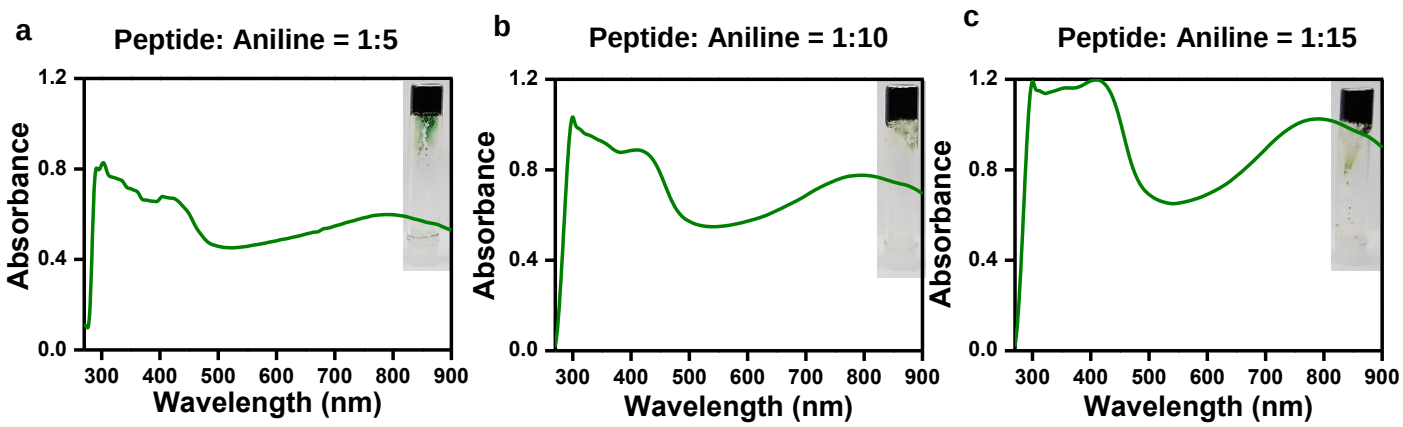

Figure S15. **UV-Vis spectra of the composite hydrogel of Fmoc-Lys(Fmoc)-Asp and PAni at different molar ratios of peptide and Ani (**Inset: digital images of the composite hydrogels. The dark green colouration of the hydrogels indicate the formation of PAni).

Note S3

The peaks centred at ~300, 412, and 800 nm corresponds to π-π*, polaron-π*, and π-polaron transitions of PAni chains. These results indicate the presence of highly conducting emeraldine salt form of PAni in the hydrogels.[33] Moreover, the doping ability of the peptide is also attested here.

Supporting References

[1] J. Schaefer, E. O. Stejskal, *J. Am. Chem. Soc.* **1976**, *98*, 1031.

[2] M. G, W. X, S. S. O, *J. Magn. Reson. Ser. A* **1994**, *110*, 219.

[3] B. M. Fung, A. K. Khitrin, K. Ermolaev, *J. Magn. Reson.* **2000**, *142*, 97.

[4] R. Zhou, X. Huang, C. J. Margulis, B. J. Berne, *Science* **2004**, *305*, 1605.

[5] P. W. J. M. Frederix, R. V. Ulijn, N. T. Hunt, T. Tuttle, *J. Phys. Chem. Lett.* **2011**, *2*, 2380.

[6] C. Guo, Y. Luo, R. Zhou, G. Wei, *ACS Nano* **2012**, *6*, 3907.

[7] M. J. Abraham, T. Murtola, R. Schulz, S. Páll, J. C. Smith, B. Hess, E. Lindah, *SoftwareX* **2015**, *1–2*, 19.

[8] D. H. De Jong, G. Singh, W. F. D. Bennett, C. Arnarez, T. A. Wassenaar, L. V. Schäfer, X. Periole, D. P. Tieleman, S. J. Marrink, *J. Chem. Theory Comput.* **2013**, *9*, 687.

[9] T. Darden, D. York, L. Pedersen, *J. Chem. Phys.* **1993**, *98*, 10089.

[10] M. Parrinello, A. Rahman, *J. Appl. Phys.* **1981**, *52*, 7182.

[11] S. Páll, B. Hess, *Comput. Phys. Commun.* **2013**, *184*, 2641.

[12] C. Guo, Z. A. Arnon, R. Qi, Q. Zhang, L. Adler-Abramovich, E. Gazit, G. Wei, *ACS Nano* **2016**, *10*, 8316.

[13] L. Schrödinger, *PyMOL the PyMOL Molecular Graphics System*, **2010**.

[14] S. Bhattacharya, S. K. Samanta, *Chem. - A Eur. J.* **2012**, *18*, 16632.

[15] K. J. C. Van Bommel, C. Van Der Pol, I. Muizebelt, A. Friggeri, A. Heeres, A. Meetsma, B. L. Feringa, J. Van Esch, *Angew. Chemie - Int. Ed.* **2004**, *43*, 1663.

[16] N. M. Sangeetha, S. Bhat, A. R. Choudhury, U. Maitra, P. Terech, *J. Phys. Chem. B* **2004**, *108*, 16056.

[17] S. Drescher, G. Graf, G. Hause, B. Dobner, A. Meister, *Biophys. Chem.* **2010**, *150*, 136.

[18] Y. Ishihara, S. Kimura, *J. Pept. Sci.* **2010**, *16*, 110.

[19] K. Wang, J. D. Keasling, S. J. Muller, *Int. J. Biol. Macromol.* **2005**, *36*, 232.

[20] D. Khatua, R. Maiti, J. Dey, *Chem. Commun.* **2006**, 4903.

[21] A. Meister, M. Bastrop, S. Koschoreck, V. M. Garamus, T. Sinemus, G. Hempel, S. Drescher, B. Dobner, W. Richtering, K. Huber, A. Blume, *Langmuir* **2007**, *23*, 7715.

[22] L. Carrick, M. Tassieri, T. A. Waigh, A. Aggeli, N. Boden, C. Bell, J. Fisher, E. Ingham, R. M. L. Evans, *Langmuir* **2005**, *21*, 3733.

[23] L. M. Carrick, A. Aggeli, N. Boden, J. Fisher, E. Ingham, T. A. Waigh, *Tetrahedron* **2007**, *63*, 7457.

[24] E. Protopapa, L. Ringstad, A. Aggeli, A. Nelson, *Electrochim. Acta* **2010**, *55*, 3368.

[25] F. Rodríguez-Llansola, J. F. Miravet, B. Escuder, *Chem. Commun.* **2009**, 7303.

[26] C. Berdugo, J. F. Miravet, B. Escuder, *Chem. Commun.* **2013**, *49*, 10608.

[27] Y. Tian, H. Wang, Y. Liu, L. Mao, W. Chen, Z. Zhu, W. Liu, W. Zheng, Y. Zhao, D. Kong, Z. Yang, W. Zhang, Y. Shao, X. Jiang, *Nano Lett.* **2014**, *14*, 1439.

[28] Y. Mei-Ni, N. Yan, G. He, L. Tai-Hong, Y. Fang, *Wuli Huaxue Xuebao/ Acta Phys. - Chim. Sin.* **2009**, *25*, 1040.

[29] M. J. Clemente, J. Fitremann, M. Mauzac, J. L. Serrano, L. Oriol, *Langmuir* **2011**, *27*, 15236.

[30] M. J. Clemente, P. Romero, J. L. Serrano, J. Fitremann, L. Oriol, *Chem. Mater.* **2012**, *24*, 3847.

[31] X. Du, J. Zhou, J. Shi, B. Xu, *Chem. Rev.* **2015**, *115*, 13165.

[32] P. Bairi, B. Roy, A. K. Nandi, *J. Phys. Chem. B* **2010**, *114*, 11454.

[33] P. Chakraborty, P. Bairi, S. Mondal, A. K. Nandi, *J. Phys. Chem. B* **2014**, *118*, 13969.